Effect of design parameters on the properties of ultra-high performance fibre-reinforced concrete in the fresh state

E. Nguyen Amanjean, Michel Mouret, Thierry Vidal

Effect of design parameters on the properties of ultra-high performance fibre-reinforced concrete in the fresh state

E. NGUYEN AMANJEAN; M. MOURET; T. VIDAL

Université de Toulouse: UPS, INSA, LMDC (Laboratoire Matériaux et Durabilité des Constructions); 135, avenue de Rangueil; F-31077 Toulouse cedex 4, France

Highlights

- Effect of design factors on the flowability of Ultra-High Performance Fibre-Reinforced Concrete
- Significant relationships exist between workability parameters and rheological ones
- Metakaolin, MK, increases viscosity and thixotropy at given fibre and paste contents
- MK mixture with the highest volumes of paste and fibres is the most thixotropic
- A practical solution is proposed for two-layer casting in precast factory context

Abstract

The properties of Ultra-High Performance Fibre-Reinforced Concrete (UHPFRC) in the fresh state were studied and analysed. The design parameters were the nature of the mineral admixture (metakaolin or silica fume), the fibre content and the paste content. Workability tests (mini slump-flow and mini L-box) were carried out immediately after mixing and after different resting times. Rheological tests were performed in order to evaluate the shear-dependent properties as well as the time-dependent ones. Workability results showed that the self-compacting ability targeted at the end of mixing was maintained up to 20 minutes after mixing for all UHPFRCs. Highlighting some significant relationships between workability measurements and rheological parameters enabled the flow properties to be analysed depending on the mixture composition. In particular, at given fibre and paste contents, UHPFRC incorporating metakaolin displayed higher plastic viscosity and structuration rate than UHPFRC containing silica fume. Furthermore, even if designed with lower fibre content or lower paste content, UHPFRC made with metakaolin was always more thixotropic than UHPFRC with silica fume. For the case of UHPFRC, having the highest metakaolin and fibre contents, a practical solution is proposed to prevent distinct-layer casting from occurring in the precast factory.

Keywords: Ultra-High Performance Fibre-Reinforced Concrete, workability, static yield stress, plastic viscosity, thixotropy, metakaolin, silica fume, stiff fibre

1. Introduction

Ultra-High Performance Concrete without fibres (UHPC) or with fibres (UHPFRC) are cementitious materials having exceptional mechanical properties characterized by a compressive strength higher than 150 MPa and an excellent durability [1]. To reach such properties, the UHP(FR)C matrix is generally composed of large amounts of cement, silica fume, fine sand, steel fibres, and a high-range water reducer (HRWR) [1-2]. Thanks to their excellent performances, UHPFRCs have been more often applied in recent years, especially in Europe, North America, and Japan. Recently, two French standards, one on the specifications of UHPFRC materials [3] and the other dealing with suitable design methods [4] were published to improve and promote knowledge of these concretes for engineers, architects and construction managers. However, the high Portland cement content and the incorporation of significant amount of silica fume and metal fibres in UHPFRC imply environmental impact and high material costs, respectively. Considering in addition the potential heat treatment applied on structural elements, it is clear that the application of UHPFRC is restricted to some exceptional structures: bridges, buildings, structural strengthening and building retrofitting. Recent research presented through UHPC reviews [5-6] have focused on mixture design methods, in particular to attenuate the drawbacks mentioned above, mainly by partial or total replacement of Portland cement and silica fume by by-products.

An analysis of the literature shows that studies have been preferentially conducted on UHPC and UHPFRC mixtures and hardened state characteristics, whereas very few deal with the properties in the fresh state [7]. It is well known that the rheological properties and thixotropic aspect of fresh concretes can be affected by the mix design parameters such as the content and nature of binder, superplasticizer, fibres, size and shape of particles, and mixing conditions [8-11]. In the case of UHPFRC, the large amount of superplasticized cement paste, which potentially provides the self-compacting ability [12], and the presence of fibres may have a strong impact on flowability. Some studies have shown that the addition of fibres in normal concrete decreases the workability [13-16]. This effect is accentuated as the fibre volume fraction and their aspect ratio increase [15-16]. In the case of UHPFRC, Martinie et al. [17] have shown the existence of a critical fibre content leading to a very strong increase in the yield stress. The maximum proportion of fibres in the mixture can be estimated as a function of the aspect ratio of the fibres, the packing fraction of sand, and the dense packing fraction of the sand in the

mixture. In addition, the self-compacting ability of UHPFRC can be associated with its thixotropic behaviour [8, 9, 18], i.e. the material is prone to build up an internal structure at rest, which can be broken after a longer time of mixing or flowing. Thixotropy can have positive effects, such as decreasing the formwork pressure and improving the stability of self-compacting concrete [19]. However, it could induce the creation of an interface, called distinct-layer casting [9]. If a first layer rests and builds structure before the next layer is cast, the yield stress increases above a critical value and a weaker interface is created [8-9]. This interface corresponds to a local structural heterogeneity characterized by higher porosity, which can facilitate the penetration of aggressive agents and can cause a loss of bending capacity of 40% [9]. Even if UHPFRC structural elements, such as bridge decks slabs, footbridges, and prestressed beams, can be thin thanks to high concrete strengths, they often require a significant volume of concrete and multi-layer casting is thus inevitable. In such a configuration, it is necessary to assess the recovery time between two successive castings related to potential distinct-layer casting problems caused by thixotropy. In particular, the total mixing time of UHPFRC can be up to 25 minutes according to Mounanga et al. [20]. Bonneau and Vernet [21] have observed that UHPFRCs present a highly thixotropic character and that their fresh properties change in time, but their study did not investigate this aspect in depth. However, the knowledge of flow properties and thixotropy of these materials means that relevant practices are needed in both the mixing and casting phases - for the concrete precast industry and for on-site applications.

The present study deals with the rheological properties of four UHPFRC mixes in the fresh state. Like the majority of these materials, the reference mix incorporates silica fume. A second mix is the same as the reference mixture but with the silica fume replaced by metakaolin (MK) since recent research has shown that this mineral additive can be considered as a possible alternative. Besides its lower cost and higher availability, MK leads to almost equivalent mechanical properties when incorporated in UHPC [22]. The third and fourth mixes are equivalent to the second mixture but with smaller amounts of fibres and binder, respectively. The workability is assessed through mini slump-flow test and mini L-box test (device dimensions are given in Section 2.2.2), and rheological properties (yield stress, viscosity) are determined from rheometric tests. Each test is performed after mixing and after various resting times in order to study the thixotropic behaviour. An analysis of the results allows estimating over time the influence of the mix parameters (mineral admixture nature, amounts of binder and fibres) on the flow properties of UHPFRC.

2. Materials and methods

90 *2.1 Materials and mix proportions*

91 The cement used in this study was an Ordinary Portland Cement (OPC) CEM I 52.5 PM-ES,
92 according to European Standard 197-1 [23]. It was chosen for its high mechanical performance
93 (minimum guaranteed 28-day strength of 52.5 MPa) and its low C_3A content (lower than 5%) which
94 reduces the water and superplasticizer demands and has a positive effect on the fresh and hardened
95 properties of concrete [21]. The silica fume used was an industrial by-product obtained by a filtering
96 process during the production of silicon. This material contains up to 95% of SiO_2 with very fine,
97 rounded, vitreous particles. A more economical and eco-friendly alternative solution could be to
98 substitute metakaolin (MK) for the silica fume. MK is a pozzolanic addition obtained from the
99 calcination of kaolinite clay, which is an abundant natural mineral. Its availability makes it less
100 expensive than silica fume. Moreover, for the industrial application in the context of this research
101 project, MK is a local material, the distance between the production site and the concrete precast plant
102 being less than 200 km, which reduces CO_2 emissions due to transport. MK was produced by flash
103 calcination of kaolinite clays. The geometrical shapes were characterized on 30000 metakaolin grains
104 by means of an optical microscope equipped with an automated particle characterization system. The
105 aspect ratio (width to length ratio) of MK particles is equal to 0.72 ± 0.02, which indicates that MK
106 grains have an elongated shape in comparison with silica fume particles, which can be considered as
107 perfectly spherical (aspect ratio close to 1). A polycarboxylic superplasticizer was used to adjust the
108 workability of concrete. The maximum amount of superplasticizer was fixed at 6% by weight of
109 binder. This dosage, exceeding the range applied for usual applications, resulted from the manufacturer
110 experience to avoid setting retardation and to limit segregation and bleeding that can affect the
111 mechanical performances. Local silica sand with particle sizes from 0 to 2 mm was selected. The main
112 chemical and physical properties of the cement, mineral admixtures and sand are summarized in Table
113 1 and Table 2. Short, straight steel fibres, 13 mm long and having a cross-sectional diameter of 0.2 mm
114 (aspect ratio = 65), were incorporated in the designed mixtures. They are characterized by a tensile
115 strength of 3000 MPa and a modulus of elasticity of 200 GPa. According to the criterion on the
116 deflection/fibre length ratio defined in [17] and regarding the yield stress range over time (Sections 3.2
117 and 3.3), the fibres could be considered as stiff in the UHPFRCs tested.

Table 1.Chemical composition of the raw materials

Compound (wt. %)	SiO_2	Al_2O_3	Fe_2O_3	CaO	MgO	Na_2O	K_2O	SO_3	Loss on ignition
Cement	22.50	3.26	2.33	64.50	1.00	0.11	0.23	2.37	1.37
Metakaolin	65.90	25.10	4.26	1.63	0.37	0.07	0.41	-	2.63
Silica fume	85.00	-	-	1.00	-	1.00	-	2.00	4.00
Sand	95.00	2.24	0.15	0.12	0.02	0.12	1.44	-	0.31

Table 2. Physical properties of the raw materials

Properties	**Cement**	**Silica fume**	**Metakaolin**
Specific surface area (m^2/g)	0.36*	23**	16**
Average particle size, D_{50} (µm)	15	20	28
Density (t/m^3)	3.15	2.24	2.50

* Blaine, ** BET

Table 3 shows the mix proportions of the four UHPFRCs. The first one (UHPFRC-1) is considered the reference mix as, like the majority of UHPFRC, it incorporates silica fume. The design of UHPFRC-1 was based on a mix proposed by a previous study [22] with a silica fume content corresponding to 25% by weight of cement, 2% of fibres by volume, and a water/cement ratio of 0.25. The proportion of silica fume was considered as optimal to achieve the highest packing density according to [1]. To limit the energy consumption and the costs, no heat treatment was applied. The three other concretes, UHPFRC-2 to 4, were designed with the objective of proposing less expensive and more eco-friendly materials while maintaining the mechanical and durability properties. These UHPFRCs incorporated MK in order to verify its influence on workability and its ability to replace silica fume without performance decrease. The MK/cement ratio was optimized using a wet packing method proposed by Wong et al. [24]. The aim of this experimental method was to find the proportion of MK in cement substitution that provided the best packing density and thus improved mechanical and durability characteristics. The optimized ratio obtained was 0.30, instead of the 0.25 ratio of the silica fume reference mix. This value was fixed for the three MK concrete mixes. The water content was optimized by using the method proposed by Mechling et al. [25] to take account of the water absorbed by MK. Currently, this absorbed water is not considered by the European standard for concrete [26]. However, with the low water content of UHPFRC and the significant amount of water absorbed by MK, too low a water/cement ratio could induce a decrease in workability which, in turn, could affect hardened state properties. The application of these two optimization methods for the UHPFRC designs incorporating MK, explained and detailed previously [27], led to the second design mix called UHPFRC-2. To investigate the influence of lower cost mixes and mix parameters on rheological and

142 mechanical properties, the other two concretes were composed with a lower fibre content for
143 UHPFRC-3 and a lower cement content for UHPFRC-4, since these constituents represent the most
144 expensive part of the concrete mix. UHPFRC-3 incorporated 1.5% by volume of steel fibres. Compared
145 to the other mixtures, UHPFRC-4 contained 22.7% less cement, and thus a binder reduction in the
146 same proportion, since the MK/cement ratio was maintained equal to 0.30. The relative packing
147 fraction of inclusions was calculated according to [17], assuming UHPFRC mixes to be suspensions of
148 stiff fibres and spherical particles of sand in cement-based paste. According to [17], a critical packing
149 value of 0.8 was identified, below which fibres and sand inclusions have little influence on the flow
150 behaviour of the mixture (mixture behaviour equivalent to paste behaviour), and above which all
151 inclusions combine and develop a continuous contact network in the suspension so that its yield stress
152 increases significantly. Then, the more the packing value close to 1, the more the mixture is firm. In
153 addition, above the packing value of 0.8, the mixture is considered to be optimized. In the present case,
154 the packing values ranged between 0.8 and 0.9, indicating that the four mixtures were correctly
155 designed and rather fluid according to [17]. The corresponding values ranged between 0.8 and 0.9,
156 indicating that the four mixtures were optimized and rather fluid. In fact, for each mixture, self-
157 consolidating ability was targeted in order to facilitate the casting of elements on site. To that end, the
158 amount of superplasticizer was adjusted to reach a required workability defined by a slump-flow value
159 of at least 30 cm (device dimensions are given in Section 2.2.2). Wille et al. [28] recommend the spread
160 values ranging from 30 to 35 cm with ASTM cone to enable self-consolidation.

161 **Table 3. Proportions by cement weight of concrete mixture with silica fume and metakaolin –**
162 **entrapped air void and characteristic compressive strength**

Materials	UHPFRC-1	UHPFRC-2	UHPFRC-3	UHPFRC-4*
Cement CEM I 52.5 (C)	1	1	1	0.773
Silica fume (SF)	0.25	-	-	-
Metakaolin (MK)	-	0.30	0.30	0.30
Sand 0/2 mm (S)	1.02	1.02	1.09	1.62
Superplasticizer (weight percentage of binder)	0.045	0.050	0.048	0.060
Steel fibres (%volume)	2.0	2.0	1.5	2.0
Effective Water/Binder	0.205	0.175	0.163	0.226
Entrapped air void**(%)	3.0	2.7	3.0	3.0
Characteristic cylinder compressive strength at 28 days (MPa)	150	152	132	132

* For UHPFRC-4, the components are calculated as a percentage of the cement content of this mix, whereas the cement content of this mix is calculated as a percentage of that of the reference mix UHPFRC-1

** Measurement in accordance with EN 12350-7 [29]

As expected, entrapped air void values were less than those measured in the case of less flowable UHPFRC (spread values ranging from 10 cm to 20 cm) [30], and similar to those obtained for fluid UHPFRC, such as the Ductal® product range [31].

The compressive strength tests were performed on 6 cylinders of nominal dimensions Ø110 mm x 220 mm at 28 days, following the specifications of the French standard code [3]. The samples were previously stored in a 20 °C, 95% RH room from demoulding until testing. From the mean values, characteristic compressive strengths (Table 3) were calculated taking the value of the Student's coefficient into account, which was equal to 2.015 for 6 samples, in accordance with the French standard [3]. The four mixes were UHPFRC according to French standard, since their compressive strengths were higher than 130 MPa. With a characteristic compressive strength equal to and slightly above 150 MPa, the UHPFRC-1 and UHPFRC-2 mixes can be used for structural applications, unlike the other two, which should be limited to architectonic uses, for instance.

2.2 Mixing and characterization in the fresh state

2.2.1 Mixing and preliminary remarks

Each 8-litre batch was prepared with a mixer equipped with a planetary beater blade and a scraper blade rotating near the wall of the bowl to avoid dead zones. The mixing sequence adopted in order to achieve good homogeneity of the mixture was as follows:

- Low speed mixing (100 rpm) of solid materials for 2 minutes;
- Addition of water and HRWR, and high speed mixing (320 rpm) for 8 minutes;
- Addition of fibres and low speed mixing (100 rpm) for 2 minutes.

Immediately after mixing and after a given resting time, two types of tests were carried out, workability tests (mini slump-flow and mini L-box tests, Section 2.2.2) and rheological tests (Section 2.2.3).

It is important to note that these tests were performed within a period of 30 min from the moment when cement and water came into contact. It is accepted that, during this period, the irreversible built-up of the microstructure of concrete can be disregarded [8, 32]. Moreover, this interval of time is chosen according to the period between the casting of two layers in a precast factory, when the second batch mixing starts immediately after the release of the first batch in the concrete hopper.

It is also important to mention that a batch was made specifically for a given concrete and a given time of measurement, so that all tests were carried out with a sample left at rest from the end of mixing (placing) until the time of measurement in the case of workability tests (rheological tests). Each test was performed at 0, 10, 15 and 20 minutes after mixing.

2.2.2 Workability tests

The flowability of UHPFRC was studied using the mini slump-flow test and the mini L-Box test as shown in Figure 1.

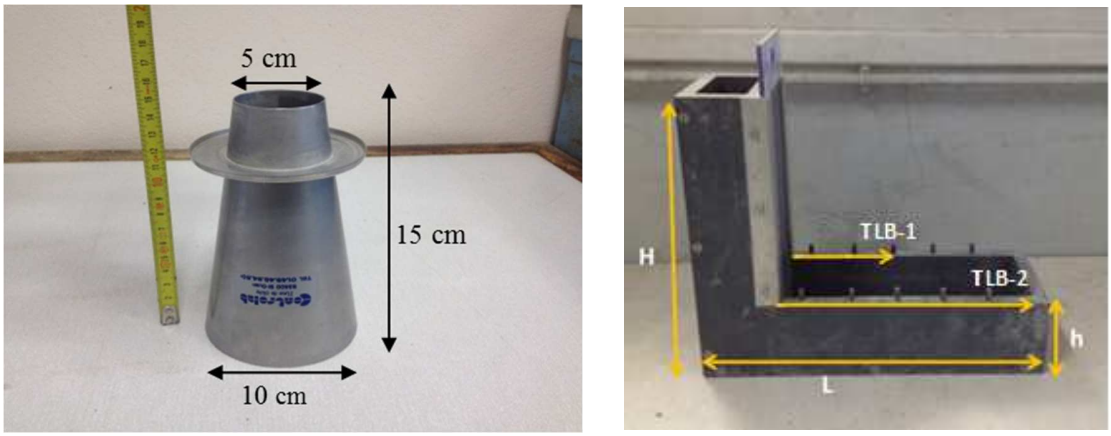

a) Mini slump cone b) Mini L-box

Figure 1. Mini slump cone and L-box test

The mini slump cone was based on the Abrams cone, used for measuring the workability of concrete according to standard EN 12350-2 [33]. The dimensions of the mini cone (Figure 1a) were 1/2 of those of the Abrams cone. The slump-flow value or flow spread corresponds to the average of diameters measured in two perpendicular directions. The mini L-box test without reinforcement was used to assess the filling ability of UHPFRCs. The device was 30 cm high (H), 36 cm long (L), and had a smaller height (h) of 7.5 cm. Such dimensions are at 1/2 scale of those of the L-box habitually used to

test self-compacting concrete. As soon as the trap separating the vertical part from the horizontal part of the L-box was lifted, flow times TLB-1 and TLB-2 were recorded when the concrete front reached half and the end of the horizontal part, respectively (Figure 1b).

Once the rest time had elapsed, samples were gently taken from the mixing bowl and placed in the cone and in the L-box. Both tests were carried out immediately after placing in a room at 20 °C ± 2 °C and no vibration was used during the tests.

2.2.3 Rheological tests

The characterizations of the rheological behaviour in steady state flow and the thixotropic aspect of UHPFRC were possible with a mortar and concrete rheometer developed by CAD Instrumentation (Figure 2a). The device is based on the shear Couette flow, where the outer cylindrical vessel is fixed while the inner tool rotates. It operates at controlled rotational speed and measures the torque necessary to shear a 2-litre sample of fresh concrete at a defined number of revolutions. To avoid slip, the inner rotating bob was a four-blade vane (Figure 2b), dragging a cylindrical block of concrete. The vane (95 mm in diameter and 56 mm in height) was first engaged on the motor shaft and then the empty stator was engaged. Next, the material was poured into the stator, so that the vane was totally immersed and centred in the sample volume. The gap width between the vane and the cylindrical container was sufficient (32.5mm) in comparison with the maximum size of sand particles (2mm) and was questionable with respect to the fibre length (13mm) as the maximum dimension of the suspension. Nevertheless, during shearing, fibres tended to align in the direction of flow, due to the wall effect and the rotating movement of the vane. Accordingly, it is unlikely that fibres would form a continuous network perpendicular to the flow throughout the gap width, which allows the medium to be considered infinite.

The measurements were performed at different effective resting times defined as the difference between the age of the material (10, 15 and 20 minutes after mixing) and the placing duration in the stator of the rheometer immediately after mixing (3 to 4.5 minutes on average). In that way, the effective resting time was considered to be zero when each mix was studied immediately after placing in the stator. It is important to recall that a sample from a new batch was tested for each concrete at a given resting time in order to assess its structuration capacity starting from the same shear history (mixing and placing) at the end of placing in the stator. In addition, during each resting time, the top of the stator was covered by a wet cloth so that evaporation was avoided. The measurements were carried out at ambient temperature, 20 °C ± 2 °C, and no vibration was used during the tests.

a) Rheometer CAD

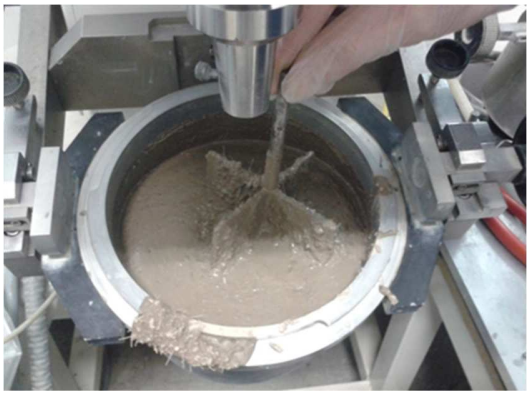

b) Cylindrical stator filled with UHPFRC and four-blade vane

Figure 2. Illustration of the rheometer used and shearing geometry

Once the yield stress is exceeded, fibres can align under the effect of the stator wall and during the rotating movement of the vane and, consequently, the flow properties of the mixes are shear-dependent. Then, each concrete sample was subjected to the same shear history, which was composed of three stages as shown in Figure 3.

During the first stage (1), the rotational velocity was maintained at 1 rpm in order to quantify the maximum stress before flowing, i.e. the static yield stress τ_S. The determination of τ_S at different resting times enabled the thixotropy of the studied concretes to be evaluated (section 3.4), based on Eq. (1):

$$\tau_S = \frac{T_S}{\left(2\pi {R_i}^2 H + \pi {R_i}^3\right)} \quad (1)$$

where T_S is the maximum measured torque at 1 rpm, R_i and H are the radius and the height of the shearing vane, respectively. Eq.(1) assumes a linear distribution of the shear stress at the top and the bottom of the vane. During this first stage, the fibre orientation had not yet occurred, according to [17].

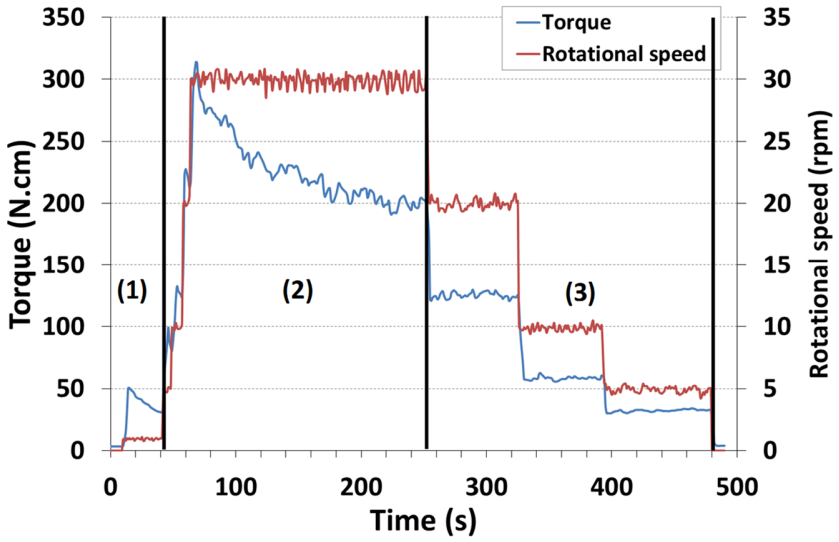

Figure 3. Typical shear history applied to UHPFRC

During the second stage (2), the rotational speed was rapidly increased to 30 rpm and maintained at this speed for at least 150 s in order to break down the time-dependent structure of the mixture [32]. In addition, the value of 30 rpm was chosen from preliminary studies as an upper limit to avoid shear-induced fibre clusters migrating on the free surface of the sample, due to secondary axial flow, which became more and more marked with the increase in the rotational speed.

Finally, during the last stage (3), the speed was decreased by steps, successively to 20 rpm, 10 rpm and finally 5 rpm, in order to determine the average of stress related to the viscous properties of concrete. The change in the speed was made after at least 60s, as soon as the variation in torque was less than or equal to 2 N.cm, assuming a steady-state flow. From the averages of Torque T_j and corresponding rotational speed Ω_j at steady state flow, the shear stress τ and the shear rate $\dot{\gamma}$ could be deduced. Each value τ_j exerted on the vane was calculated using Eq. (1). A characteristic shear rate, $\dot{\gamma}_j$, at the vane was calculated according to Eq. (2) [34]:

$$\dot{\gamma}_j = \max\big((Eq3);(Eq4)\big) \tag{2}$$

$$\dot{\gamma}_j = 2T_j\frac{d\Omega}{dT} \tag{3}$$

$$\dot{\gamma}_j = \frac{2T_j\frac{d\Omega}{dT}}{1-\left(\frac{R_i}{R_e}\right)^2} - \frac{\Omega_j - T_j\frac{d\Omega}{dT}}{ln\left(\frac{R_i}{R_e}\right)} \tag{4}$$

where R_e is the radius of the cylindrical vessel.

The maximum value (Eq. (2)) was considered as the appropriate value maximizing the energy dissipation in the sheared sample.

Here, the derivative $d\Omega/dT$ was calculated from the fitting of the set of data (T_j; Ω_j) by considering the Herschel-Bulkley model (Eq. (5)):

$$T = T_0 + K\Omega^m \quad (5)$$

where T_0, K and m are numerical parameters identified by the least squares method for each concrete.

It is worth noting that Eq. (1), Eq. (3) and Eq. (4) are rigorously valid for the cylindrical Couette geometry. In the case of the vane tool, cylindrical flow can be accepted with sufficient accuracy at low shear rates [35], i.e. for the determination of τ_s by means of Eq.(1). At higher shear rates, Eq.(3) and Eq.(4) are questionable because a yield stress material does not flow in a really cylindrical layer near the blades of the vane. That is why the radius of the vane R_i was replaced by an equivalent inner radius $R_{i,eq}$ in Eq.(4) in order to consider the radius of the inner cylinder of a Couette geometry that would develop the torque T_j at the rotational speed Ω_j as measured in the vane geometry [36]. The value of $R_{i,eq}$ was determined experimentally from preliminary measurements on Newtonian fluids.

Moreover, Eq. (4) is usable provided that the Bingham approximation is correct. This approximation can be assumed for the UHPRCs studied because the exponent m in Eq. (5) was found to be close to 1 and previous studies had shown that the observed linear relationship in the macroscopic plane (T; Ω) was conserved in the local plane (τ; $\dot{\gamma}$) [37-38]. Figure 4 confirms the linear relationship in the plane (τ; $\dot{\gamma}$) when applying Eq. (3) and Eq. (4). For each concrete, the line through the experimental points was constructed in 2 steps:

1) The stress corresponding to $\dot{\gamma} = 0s^{-1}$ was deduced from the parameter T_0, using Eq. (1).
2) Starting from the value determined in step 1, the slope of the line, i.e. the plastic viscosity η_p, was identified by the least squares method.

Through the typical examples shown in Fig.4, the shear rate ranged from 1.5 s^{-1} to 7.5 s^{-1} for all the mixes investigated, which is in accordance with the 1 to 10 s^{-1} shear rate range encountered in their context of placing by pouring [8]. Since Grünewald has shown that fibres are rarely randomly oriented in self-compacting fibre reinforced concrete after classical placing operations [15], it can be assumed that the fibre orientation during the rheological measurements was not really a bias but was, to some extent, representative of the context of fluid UHPFRC placing in a precast factory.

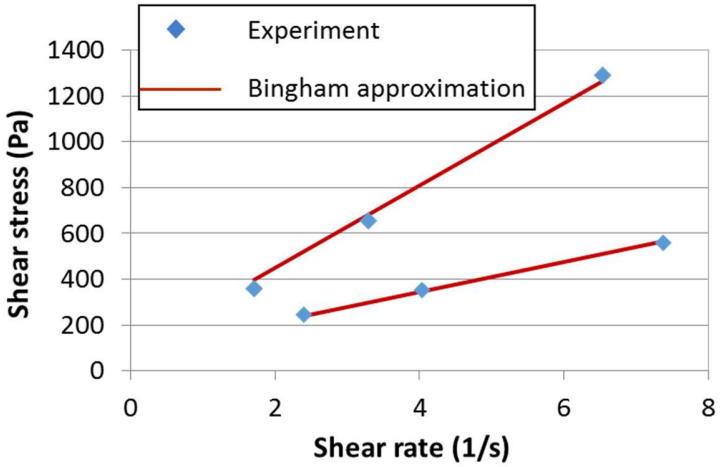

Figure 4. Typical examples of Bingham approximation applied to UHPFRC

3. Results and discussion

3.1 Correlation between flow properties

In order to analyse the results discussed in Sections 3.2 and 3.3 and highlighting the specificity of each mix studied, the degree of correspondence between two flow properties was first assessed by using the Kendall rank correlation coefficient *"tau"* (Eq. (6)) which is insensitive to an utmost point in the scatterplot and does not need a hypothesis on the normality of the parameters studied:

$$tau = \frac{\sum concordant\ pairs - \sum discordant\ pairs}{Total\ number\ of\ possible\ pairs} \quad (6)$$

where

concordant pairs correspond to a simultaneous increase in the properties between two paired observations,

discordant pairs correspond to an increase in one property and a decrease in the other between two paired observations.

Based on Eq. (6), *tau* ranges from -1 to +1, a positive value indicating that the ranks of both properties increase together, while a negative value means that, as the rank of one property increases, the rank of the other decreases. In the present study, 16 values were considered for each property (4 mixes and 4 resting times). Table 4 gathers together the values of *tau*. The existence of a correlation was tested at a significance level of 0.01. Accordingly, each calculated *tau*-value had to be equal to or greater (in absolute value) than the threshold value defined in the reference tables (see [39] for example).

Table 4. Kendall correlation coefficient values to assess relationships between flow properties

	τ_s	η_p	Spread	TLB-1	TLB-2
τ_s	1.000				
η_p	0.427	1.000			
Spread	**-0.712**	-0.380	1.000		
TLB-1	**0.843**	0.407	**-0.730**	1.000	
TLB-2	**0.644**	**0.700**	-0.462	**0.644**	1.000

Values in bold indicate significant correlations for which tau is greater than the critical value (0.483) at the 0.01 significance level.

As shown in Table 4 and by Fig.5a, a correlation is found between the static yield stress τ_s and the spread measured during the mini slump-flow test, as expected, and confirms previous results obtained on cement pastes and concretes [40]. Also, a significant relationship is observed between τ_s and the time to reach the half way distance of the horizontal part in the L-box test, *TLB-1* (Fig.5b) and, to a lesser extent, with the time to reach the end of the horizontal part of the L-box, *TLB-2*. The plastic viscosity η_p is only correlated with TLB-2 (Fig.5c), although the relationship is more dependent on the nature of the mix.

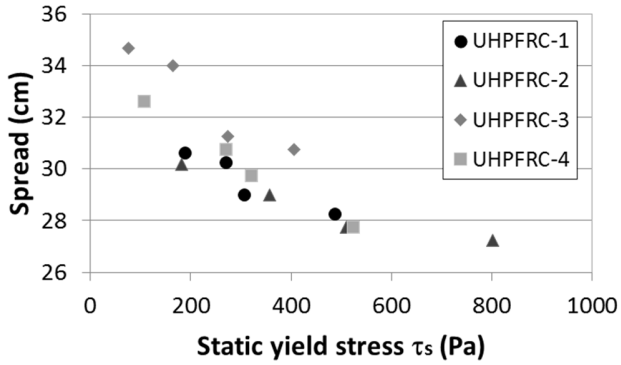

(a)

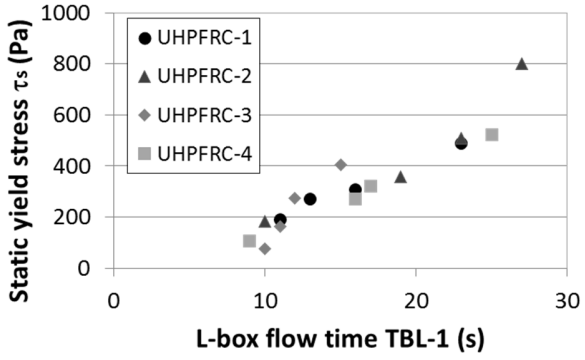

(b)

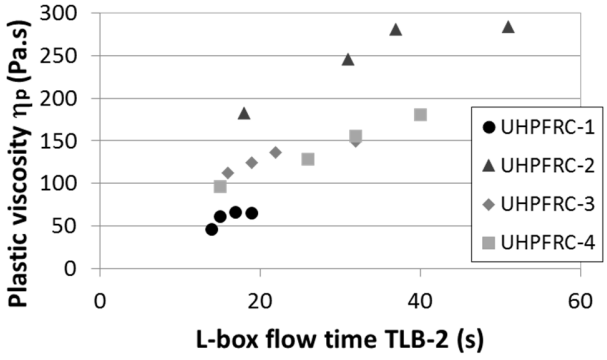

(c)

Figure 5. Relationships between the slump-flow spread and the static yield stress (a), the flow time TLB-1 and the static yield stress (b), and the flow time TLB-2 and the plastic viscosity (c)

3.2 Flow properties immediately after mixing

Mini slump-flow spread and mini L-box flow time measurements were performed for each resting time. The results of these measurements immediately after the mixing (t_0) are presented in Figure 6. From repeatability tests, the experimental uncertainties are ±0.5 cm and ±0.5 s for spread values and L-box time values, respectively.

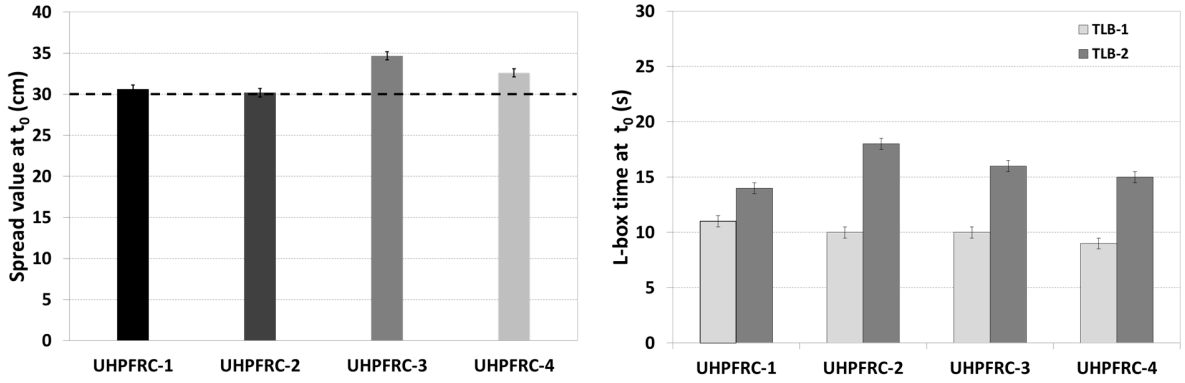

Figure 6. Slump-flow spread value and L-box flow time value at the end of mixing, t_0

Spread values of all UHPFRCs are between 30 cm and 34 cm, thus meeting the target value, greater than or equal to 30 cm. All UHPFRCs have a self-compacting capacity immediately after mixing, enabling casting without vibration. The slump-flow value is slightly higher for UHPFRC-3, characterized by a lower fibre content which reduces inter particles friction and improves the flowability compared to other UHPFRCs. This result is in agreement with several studies [13-17] that observed a decrease in slump values when fibres were incorporated in self-compacting concrete, in normal concrete, and also in UHPC. This phenomenon is accentuated when the fibre content increases.

At the end of mixing, t_0, the L-box flow time parameters *TLB-1* and *TLB-2* present different evolutions, depending on the properties of flow. When *TLB-1* is measured, there is a transient flow governed by both the material structure existing at the onset of the test and linked to the yield stress, and the viscous properties. The interaction implies that the values of *TLB-1* are not very different in any of the concretes studied. In contrast, the flow tends to arrive at a steady state a little more when *TLB-2* is measured, so viscosity becomes the main parameter affecting the *TLB-2* values (see Table 4), and differences are visible at t_0: *TLB-2* value is lower for UHPFRC-1 than for UHPFRC-2 containing metakaolin (MK). This result can be explained by the round shape of the silica fume grains, which facilitated the flow, compared to the angular form of MK particles. This aspect will be discussed

354 further in Section 3.3. The maximum flow time is obtained for UHPFRC-2, which has the highest
355 content of fibres and MK, with respect to UHPFRC-3 and UHPFRC-4 respectively.

356 The values of the static yield stress, τ_s, and the plastic viscosity, η_p, at t_0 are reported in Table 5.
357 Based on Eq. (1), the mean relative uncertainty of τ_s is 3%. Considering the variation in torque of 2
358 N.cm at steady state flow, the average coefficient of variation on the regression for the determination of
359 η_p is 5%.

360 **Table 5. Static yield stress and plastic viscosity at t_0**

	Static yield stress (τ_s) in Pa	Plastic viscosity (η_p) in Pa.s
UHPFRC-1	188	46
UHPFRC-2	182	182
UHPFRC-3	76	112
UHPFRC-4	107	96

361 Static yield stresses τ_s obtained immediately after mixing varied from 76 to 188 Pa. These values
362 are higher than those obtained by Roussel and Cussigh [9] for self-compacting concrete, SCC (48 to 70
363 Pa). There were distinct experimental conditions (slight variations in the vane dimensions and in the
364 imposed rotational speed of the vane tool), and distinct hypotheses on the stress distribution (constant
365 in [9], linear here) at the bottom and top of the vane between the two studies. However, the difference
366 can be mainly attributed to the greater volume of paste in UHPFRC [41] than in SCC and to the
367 incorporation of fibres in UHPFRC. The two first mixtures, which have the same fibre content and an
368 almost equivalent volume of paste, have similar τ_s values. It is worth noting that the high τ_s value
369 measured when silica fume is incorporated (UHPFRC-1) confirms the well-known effect of silica fume
370 to increase the cohesiveness of the mixture [42]. A decrease in the value of this parameter is noted for
371 UHPFRC-4, which is characterized by the lowest paste volume. The minimum value of the static yield
372 stress is obtained for UHPFRC-3 with its lower fibre content. As fibres participate in the development
373 of an internal network in concrete, they increase the yield stress [43]. Hence, a lower fibre content in
374 UHPFRC-3 can be related to a moderate yield value.

375 The values of plastic viscosities are strongly dependent on the mix compositions. UHPFRCs
376 incorporating metakaolin (MK) have higher plastic viscosities, ranging broadly from 100 Pa.s (upper
377 limit for SCC [44]) to 200 Pa.s (upper limit specified in some high strength concrete applications [45]).
378 Even if viscosity increases with the superplasticizer content [46] through a steric effect, and with the
379 incorporation of stiff fibres through particle interaction and packing density loosening [43], the
380 UHPFRCs studied here present relatively moderate plastic viscosity values by two aspects: (1) the use

of rolled sand as aggregate, which reduces friction, and (2) the great volume of ultrafine particles that separate the aggregates from each other, and therefore limit intergranular friction. Moreover, because ultrafine particles are round (silica fume), the intergranular friction is even more moderate and the plastic viscosity is significantly lower for UHPFRC-1.

The results of flow time (when measured at the end of the L-box, where flow is mainly controlled by the viscous properties) and plastic viscosity demonstrate that UHPFRC-1 with silica fume is characterized by a better flowability than the other mixes with MK.

3.3 Flow properties after different resting times

The spread values and the flow times after different resting times are shown in Figure 7 for each UHPFRC.

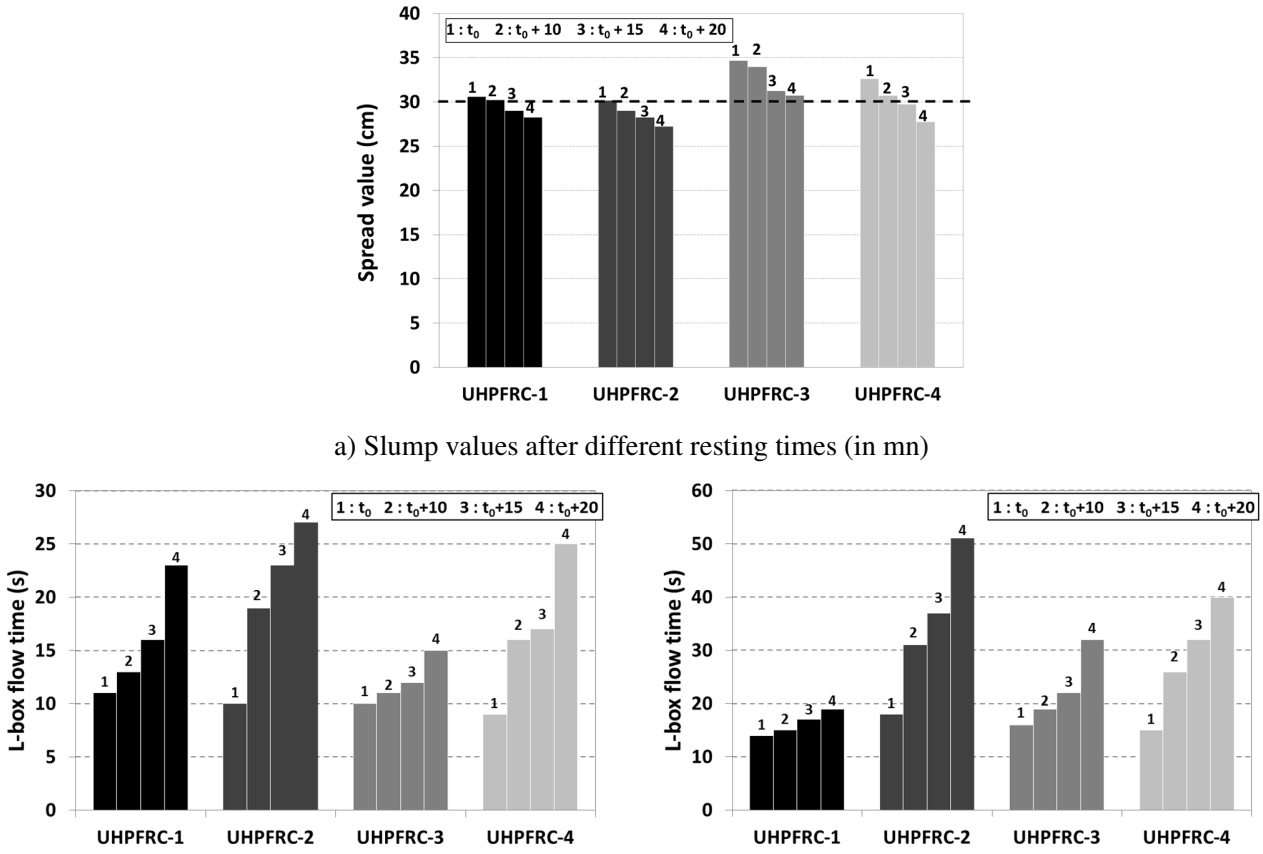

a) Slump values after different resting times (in mn)

b) Flow time values after different resting times: *TLB-1* (left) and *TLB-2* (right)

Figure 7. Evolution of slump value and flow time over time

In Figure 7a, the minimum targeted value of 30 cm is indicated by the dotted line. The slump values decrease at increasing resting time, revealing a loss of workability. However, the reduction remains

394 small during the 20 minutes counted from the end of the mixing; in this period, the self-compacting
395 ability is maintained.

396 Both *TLB-1* and *TLB-2* increase with resting time for all concretes (Figure 7b), indicating a loss of
397 workability over time, as previously observed for spread values (Figure 7a). Regarding *TLB-1*,
398 governed rather by the internal structure of the material (Section 3.1, Table 4), the most moderate
399 increase is shown in the case of UHPFRC-3, which has the lowest fibre content. In contrast, the
400 evolution of TLB-2 depends on the modification over time of the inter-particle rearrangement during
401 the flow. The nature and the particle shape of the mineral admixture control the rearrangement because,
402 as first order parameter, it controls the packing at rest of the suspension and the superplasticizer-binder
403 interaction varying over time. The increase remains low for UHPFRC-1 with silica fume, whereas it is
404 more marked for the other concretes with MK. Accordingly, when flow tends to be in steady state and
405 governed by the viscous properties of the material, the inter-particle frictions in the material are limited
406 by the round-shaped particles of silica fume in comparison with the more angular form of MK. For the
407 latter, the arrangement of particles induced in the suspension can imply residual water absorption
408 altering flow over time. Hence, it is no wonder that concretes incorporating both high fibre and MK
409 contents (cases of UHPFRC-2 and UHPFRC-4) also exhibit the most significant increase in both *TLB-1*
410 and *TLB-2* after as little as 10 minutes of rest.

411 Figure 8 presents the variations of the static yield stress and the plastic viscosity according to the
412 time of the test after mixing.

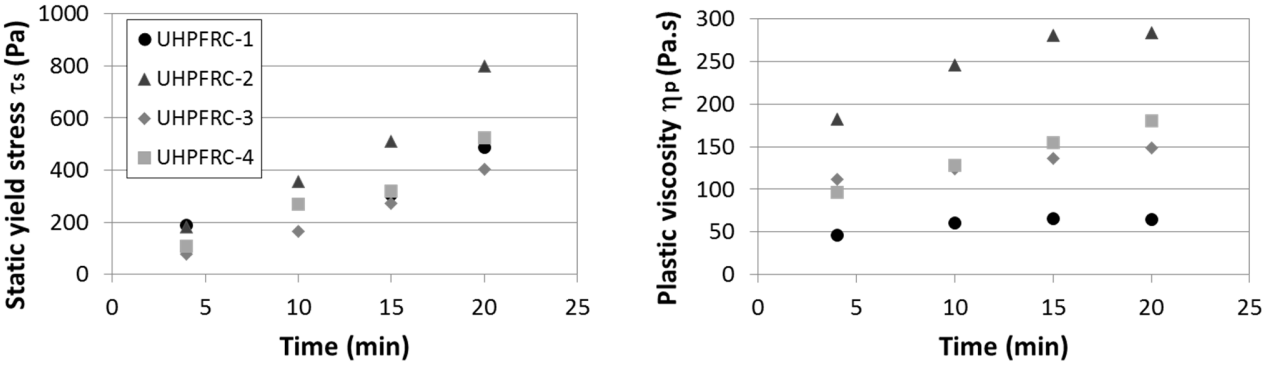

413 **Figure 8. Evolution of the static yield stress (left) and the plastic viscosity (right) over time**

414 An increase in the static yield stress τ_s over time is observed for all concretes, expressing a
415 structuration capacity and the loss of workability when concretes stay at rest. These results are in
416 agreement with those of mini slump-flow tests. The comparison among the concretes shows that

417 UHPFRC-2 has the highest τ_s value whatever the time of test, but especially beyond 15 minutes. The
418 lowest value is obtained for UHPFRC-3, which contains a smaller fibre volume fraction, in agreement
419 with observations made on the variations of flow time *TLB-1* over time, as expected from the
420 relationship highlighted between τ_s and *TLB-1* (Table 4). The reduction of paste volume in UHPFRC-3
421 also decreases the static yield stress value.

422 Concerning the plastic viscosity, UHPFRC-1, with silica fume, presents the lowest values and a
423 very slight increase with time, unlike UHPFRCs incorporating MK. These results confirm the analysis
424 of the flow time values *TLB-2*, considering the significant correlation with the plastic viscosity (Section
425 3.1). The distinct viscosity evolution over time related to UHPFRC-1 in comparison with mixes
426 incorporating MK can be attributed to the difference in particle shape between MK and silica fume. It
427 is well established that the flow of cement-based materials is improved when silica fume is used,
428 thanks to its regular round shape, which reduces the friction between grains, provided that the use of
429 superplasticizer ensures de-flocculation; see for example [42, 46]. In contrast, the irregular flat shape of
430 MK can induce higher values of viscosity [41, 46, 47]. The comparison between the three UHPFRCs
431 with MK show that the plastic viscosity depends on fibre and MK contents. UHPFRC-2, containing the
432 greatest amounts of fibres and MK was characterized by the highest plastic viscosity of all mixes at all
433 testing times.

434 *3.4 Thixotropy investigation*

435 The results presented in Sections 3.2 and 3.3 highlight the change of flow properties at increasing
436 rest times. The alteration was more or less pronounced depending on the nature of the mix. In fact,
437 when concrete is at rest, two phenomena can occur. The first one is the consequence of the evolution of
438 hydration reactions which are obviously irreversible. In our case, all measurements were performed
439 within a period of 30 minutes counted from the moment when cement and water were put in contact, so
440 the hydration phenomenon can be neglected [9, 32]. The second phenomenon is the thixotropic
441 property controlling the structuration capacity of the material. In practice, a concrete can be considered
442 thixotropic when, after mixing, rapid (during several minutes) structuration (flocculation) occurs at
443 rest, followed by very rapid (tens of seconds) de-structuration (de-flocculation of clusters of particles)
444 during ordinary placing operations such as pouring, where the velocity gradient is in the range of 1 to
445 10 s^{-1} [8]. The thixotropic character of cementitious materials depends on their composition. The origin
446 of thixotropy can be linked to the colloidal nature of such materials, especially of their finer particles

447 such as cement, mineral admixtures and fine sand. According to Wallevik [48], particles up to 20 µm
448 can be considered to be involved in the colloidal nature of cement-based materials.

449 Here, the property of thixotropy deserves to be studied in greater detail because all the mixtures tested
450 still showed measurable workability properties as soon as they were slightly reworked in the mixing
451 bowl after a given rest period, at the moment of placing in the mini-cone and the mini L-box.

452 *3.4.1 Characterization and highlighting of thixotropy*

453 One way to assess thixotropy is to plot the static yield stress τ_s versus the effective rest time
454 counted from the end of placing of a sample of UHPFRC in the stator of the rheometer (Figure 9).
455 Since τ_s can be considered as a continuous network of inter-particle bonds in plain cement-based paste,
456 it can reflect the structural build-up when its evolution with resting time is characterized. In the case of
457 UHPFRC, τ_s is not only related to the energy required to break the inter-particle bonds in the matrix
458 after a resting time, but is also related to the energy required to orientate fibres in a more stiff matrix.
459 Hence, there is a strong interaction between the fibre content and the structural build-up of the matrix.
460 In the 0.8-0.9 range of relative volume fraction of inclusions (sand and fibres) calculated according to
461 [17], it is possible that all the mixes present such a strong network of inclusions that the structural
462 build-up of the matrix itself might be slowed down [11]. In the following, the increase in τ_s over time is
463 considered as an indication of the structuration capacity of UHPFRC through the interaction between
464 the fibre content and the inter-particle bonds in the matrix.

465 It is important to recall here that, for a given mix, a new batch was made for each measurement
466 corresponding to a given resting time so that the history of any sample was the same between the end
467 of mixing and the placement in the rheometer.

468 Figure 9 shows that τ_s can be assumed to linearly increase over time ($R^2 > 0.91$ in all cases). The same
469 result was found by [9, 11, 49, 50] in the case of fibre-reinforced cement-based materials. Then, the
470 thixotropic character can be estimated through a parameter denoted A_{thix} which characterizes the
471 structuration capacity at rest. The structuration rate A_{thix} corresponds to the slope of the linear
472 relationship between τ_s and the resting times [8-9] (dotted lines in Fig. 9, which were determined by the
473 least squares method).

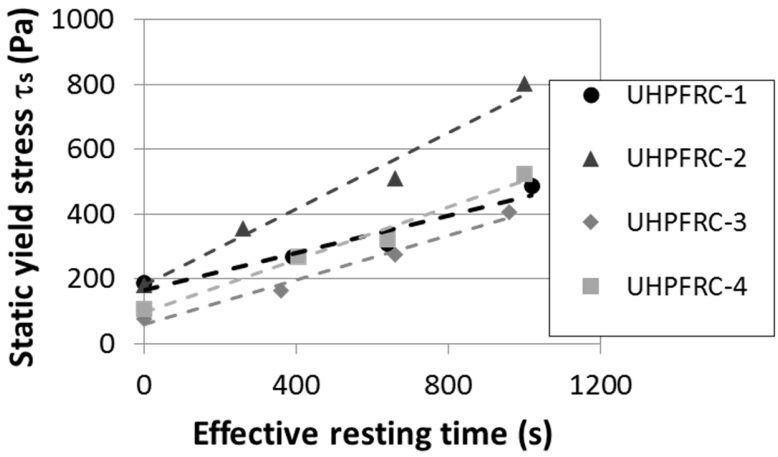

Figure 9. Evolution of the static yield stress according to the effective resting time

The values of A_{thix} are given in Table 6. The classification on thixotropy of SCC as Binghamian fluids is also included in Table 6. The comparison between the values obtained and the classification is legitimate since the UHPFRCs studied are Bingham materials in the shear rate range investigated (Section 2.2.3, Figure 4) and can be considered as self-consolidating (Section 2.1).

Table 6. Structuration rate, A_{thix}, values, classification following [8] and critical time between two concrete casting layers (h=0.1m)

Mixture	Thixotropy A_{thix} (Pa/s)	Classification	Bulk density (kg/m^3)*	Critical time (minutes)
UHPFRC-1	0.28	Thixotropic ($0.1 < A_{thix} < 0.5$)	2417	40.3
UHPFRC-2	0.57	Highly thixotropic ($A_{thix} > 0.5$)	2419	19.8
UHPFRC-3	0.34	Thixotropic ($0.1 < A_{thix} < 0.5$)	2401	33.0
UHPFRC-4	0.41	Thixotropic ($0.1 < A_{thix} < 0.5$)	2408	27.4

* Measurement in accordance with EN 12350-6 [56]

The calculated values of A_{thix} seem to be coherent when compared to those found by [8-9] in the case of SCC, with structuration rates ranging from 0.12 Pa/s to 1.14 Pa/s. The results are also consistent with another study highlighting the increase in A_{thix} as soon as SCC incorporates mineral admixtures at constant water/powder ratio, with a gravel/sand ratio and a superplasticizer content adjusted to achieve slump flow values between 630 mm and 700 mm [10]. Hence, based on the classification of SCC according to the flocculation rate presented in Table 6, all the UHPFRC mixes studied are thixotropic concretes. However, UHPFRC-1, with silica fume, is less thixotropic than UHPFRCs incorporating MK. The difference may be related to the blend composition, especially the nature and amount of ultrafine addition, and inter-particle interactions. Works on paints established as early as 1941 that

thixotropy was enhanced in systems incorporating non-spherical particles [51]. Since then, this fact has been confirmed with regard to cement-based materials. For instance, Ahari et al. [52] noted that the nature of the mineral admixture and its interactions with other fines in the mixture had an effect on the structuration rate of concrete. They showed that the use of MK in SCC accentuated the thixotropy, which increased with the MK content. Carneiro et al. [53] observed a recovery of the structure in fluid concretes containing MK with significant rounded quartz content. In the present study, the most thixotropic concrete was UHPFRC-2, containing the highest amount of metakaolin and steel fibres. This influence can be explained by the fact that the shape of MK grains is essentially platelet-type, elongated and angular. As a result, inter-particle bonds are developed at rest, thereby trapping a significant amount of water and superplasticizer. Consequently, the longer the resting time lasts, the more numerous and strong inter-particle bonds become, and the higher the static shear stress will be. The congestion effect developed by the presence of steel fibres is added to the inter-particle bonds in the matrix and they contribute to the increase in the structuration capacity. The combination of the two effects can be at the origin of the high structuration rate of UHPFRC-2 in comparison with UHPFRC-3 and UHPFRC-4.

3.4.2 Practical implications

Thixotropy can be beneficial as it reduces formwork pressure and static segregation after casting in the case of SCC [19, 49, 54, 55, 57]. However, Roussel [8] and Roussel et al. [9] point on the risk of material heterogeneity in case of multi-casting as a major disadvantage of the thixotropy. During placing, if a layer of thixotropic SCC builds structure at rest before a second layer of concrete is cast on top of it, the two layers can then fail to mix, creating an interface with high porosity and permeability, which affects the mechanical strength and makes it easier for aggressive species to penetrate.

Considering the thixotropic nature (Section 3.4.1) and the manufacturing context of the UHPFRCs studied, it is important to assess the risk of distinct-layer casting. In fact, the low batch volumes in precast industry conditions associated with the long mixing time of UHPFRC most often implies multilayer casting. Thus, it appears essential to evaluate the critical time between the casting of two layers in order to avoid a local loss of mechanical and durability properties in precast elements.

According to [8], it is possible to predict the critical time, after which the two layers will not mix (Eq. (7)):

$$T_c = \frac{\rho g h}{3.5 A_{thix}} \quad (7)$$

where:

T_c is the critical time (seconds);

A_{thix} is the structuration rate (Pa/s);

h is the thickness of the second layer (m);

ρ is the density of the concrete (kg/m^3);

g is the gravitational acceleration constant (9.81 m/s²).

Eq. (7) is limited to SCC considered as Bingham material and a second concrete layer thickness greater than 10 cm. Even though UHPFRC applications usually employ thin elements, the critical time is evaluated (Table 6) in order to give information to industry on the thixotropic behaviour of the UHPFRCs studied.

The UHPFRC with silica fume is characterized by the highest critical time compared to those incorporating metakaolin. The strongest structuration rate is obtained for UHPFRC-2, inducing a lower critical time. This period is rather short compared to the total time of a production cycle on site (mixing and casting phases) (Table 7), for an element incorporating one of the UHPFRCs studied.

Table 7. Specific production cycle in the precast factory (UHPFRC is produced using a traditional pan mixer)

Actions	Time (minutes)
Weighing of materials	3
Dry mixing	2
Wet mixing	8
Wet mixing with fibres	2
Mixer emptying	1
Mixing time	16
Transportation+ casting	12
Total time	**28**

The total production time is 28 minutes which is longer than the critical times of UHPFRC-2 and UHPFRC-4. The solution of using vibration is not relevant for UHPFRC since it could disturb the fibre orientation and distribution and thus affect the tensile behaviour of precast elements. Considering the lowest value of the critical time in Table 7, it is simple to optimize the manufacturing of precast UHPFRC elements in order to prevent distinct layer concrete when multi-casting is necessary, whatever the UHPFRC design. The optimization consists in starting the following concrete batch immediately after emptying the first one into the hopper (Figure 10). In that way, the first layer will

545 have been placed for 4 minutes when the second one is emptied into the hopper. Hence, only 16
546 minutes will elapse before the two layers mix under the weight of the new concrete, which is less than
547 the shortest critical time (UHPFRC-2). It is the proposed solution taking into account the current
548 mixing means. There is no doubt that the use of high shear mixer with high mixing energy will reduce
549 the mixing time and improve the conditions for two-layer casting by reducing the time elapse between
550 the placing of both layers.

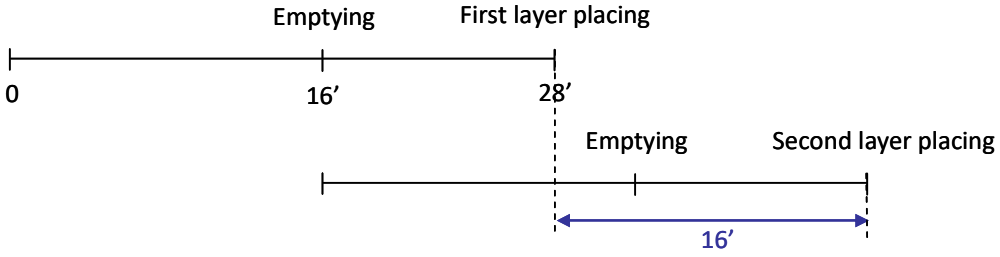

551

552 **Figure 10. Optimization of the manufacturing process in case of two-layer casting**

553 **4. Conclusions**

554 The objective of the study was to assess the flow properties of UHPFRC designed for precast
555 manufacturing, according to the nature of the mineral admixture (silica fume or metakaolin), the fibre
556 content and the cement content. Workability (mini-cone and mini L-box) and rheological tests were
557 carried out directly after mixing up to 20 minutes after mixing. Based on the experimental data
558 obtained, the following conclusions can be drawn:

559 1. The self-compacting ability targeted immediately after mixing (mini slump-flow equal to or
560 greater than 30 cm) for all mixes is not significantly altered during the 30-min period from the
561 beginning of contact between cement and water.
562 2. The Binghamian behaviour can be considered acceptable in the shear rate range investigated,
563 which corresponds to classical placing operations such as pouring.
564 3. Mini L-box flow times *TLB-1* (concrete reaches half of the horizontal part) and *TLB-2* (end of
565 the horizontal part) are significantly correlated to the static yield stress τ_s and the plastic
566 viscosity η_p, respectively. A significant relationship is also found, as expected, between the
567 mini-slump flow and τ_s.
568 4. For given fibre and paste (cement + mineral admixture + superplasticizer + water) contents, the
569 incorporation of metakaolin (MK) increases the plastic viscosity at any age of test and a higher
570 structuration rate is obtained in comparison with the use of silica fume, even though the static

yield stress is similar in both cases immediately after mixing. These results can be attributed to the difference in particle shapes. The regular, round shape of silica fume particles favours flowability and so the plastic viscosity is not significantly increased during rest. On the other hand, the irregular type and platelet form of MK particles increases i) the strength of the inter-particle bonds and the structuration capacity of the mix, and ii) friction between the particles once flow is initiated.

5. Even if the fibre content or the paste content decreases, the flat shape of MK particles remains the main factor causing the higher values of plastic viscosity, a larger increase of plastic viscosity over time and higher structuration capacity of UHPFRC incorporating MK in comparison with mixes that contain silica fume.
6. For a given metakaolin/cement ratio and whatever the age of test, i) the fibre content governs the static yield stress (the lower the fibre content, the lower the static yield stress), ii) the decrease in the paste content or the fibre content reduces the plastic viscosity to almost the same extent. Thus, the effect of the packing density of inclusions (sand, fibres) on the flow capacity of UHPFRC suspensions is of great importance, as pointed out by previous studies [11, 17].
7. All the mixes studied were thixotropic according to the classification proposed in [8] for SCC. Those incorporating MK always exhibited higher thixotropy than the mixes with silica fume. The most thixotropic MK mixture contained the highest volumes of paste and fibres. The combination of the effects of metakaolin particle shape and steel fibre friction may be the reason why this concrete mix showed the highest structuration rate.
8. The critical time estimated for all the UHPFRCs studied gives information about the maximum acceptable delay between the casting of two layers which allows preventing the formation of a weak interface corresponding to a material discontinuity that locally affects the mechanical properties. The shortest critical time (19.8 minutes) is obtained for the most thixotropic concrete with metakaolin and characterized by the highest amounts of fibres and paste. In the precast factory, considering that the estimated time required for the UHPFRC mixing sequence is about 16 minutes, including the weighing of materials, and that the total time is around 28 minutes, including transportation and casting time, the risk of creating a singular interface is very real. A practical solution with regard to logistics optimization has been proposed.

Acknowledgements

The authors are very grateful to the French precast enterprise Lagarrigue and the Association Nationale de la Recherche Technique (ANRT) for supporting the present research.

References

[1] P. Richard, M. Cheyrezy, Composition of reactive powder concretes, Cem. Concr. Res. 25(7) (1995) 1501-1511. https://doi.org/10.1016/0008-8846(95)00144-2.

[2] P. Rossi, A. Arca, E. Parant, P. Fakhri, Bending and compressive behaviours of a new cement composite, Cem. Concr. Res. 35(1) (2005) 27-33. https://doi.org/10.1016/j.cemconres.2004.05.043.

[3] NF P18-470 Concrete - Ultra-high performance fibre-reinforced concrete - Specifications, performance, production and conformity, (2016).

[4] NF P 18-710, National addition to Eurocode 2 - Design of concrete structures: specific rules for Ultra-High Performance Fibre-Reinforced Concrete (UHPFRC) (2016).

[5] E. Ghafari, H. Costa, E. Júlio, Critical review on eco-efficient ultra high performance concrete enhanced with nano-materials, Constr. Buil. Mat. 101 (2015) 201-208. https://doi.org/10.1016/j.conbuildmat.2015.10.066.

[6] C. Shi, Z. Wu, J. Xiao, D. Wang, Z. Huang, Z. Fang, A review on ultra high performance concrete: Part I. Raw materials and mixture design, Constr. Buil. Mat. (2015) 741–751. https://doi.org/10.1016/j.conbuildmat.2015.10.088.

[7] J. Dils, V. Boel, G. De Schutter, Influence of cement type and mixing pressure on air content, rheology and mechanical properties of UHPC, Constr. Buil. Mat. 41 (2013) 455–463. https://doi.org/10.1016/j.conbuildmat.2012.12.050.

[8] N. Roussel, A thixotropy model for fresh fluid concretes: theory, validation and applications, Cem. Concr. Res. 36(10) (2006) 1797-1806. https://doi.org/10.1016/j.cemconres.2006.05.025.

[9] N. Roussel, F. Cussigh, Distinct-layer casting of SCC: The mechanical consequences of thixotropy. Cem. Concr. Res. 38(5) (2008) 624-632. https://doi.org/10.1016/j.cemconres.2007.09.023.

[10] M.K. Rahman, M.H. Baluch, M.A. Malik, Thixotropic behavior of self-compacting concrete with different mineral admixtures, Constr. Buil. Mat. 50 (2014) 710-717. https://doi.org/10.1016/j.conbuildmat.2013.10.025.

[11] A. Perrot, T. Lecompte, P. Estellé, S. Amziane, Structural build-up of rigid fiber reinforced cement-based materials. Materials and Structures 46 (2013) 1561-1568. https://doi.org/10.1617/s11527-012-9997-9.

[12] J. Ma, M. Orgass, F. Dehn, D. Schmidt, N.V. Tue, Comparative investigations on ultra-high performance concrete with and without coarse aggregates, in: Proceedings of international symposium on ultra high performance concrete, Germany, (2004) 205-212.

[13] B.P. Hughes, N.I. Fattuhi, Predicting the flexural strength of steel and polypropylene fibre-reinforced cement-based beams, Composites 8(1) (1977) 57-61. https://doi.org/10.1016/0010-4361(77)90028-3.

[14] P. Rossi, Mechanical behaviour of metal-fibre reinforced concretes, Cem. Concr. Comp. 14(1) (1992) 3-16. https://doi.org/10.1016/0958-9465(92)90034-S.

[15] S. Grünewald, Performance-based design of self-compacting fibre reinforced concrete, PhD thesis, Delft University of Technology, Delft University Press (2004).

[16] H.B. Dhonde, Y.L. Mo, T.T. Hsu, J. Vogel, Fresh and hardened properties of self-consolidating fibre-reinforced concrete, ACI Mater. J. 104(5) (2007) 491.

[17] L. Martinie, P. Rossi, N. Roussel, Rheology of fibre reinforced cementitious materials: classification and prediction, Cem. Concr. Res. 40(2) (2010) 226-234. https://doi.org/10.1016/j.cemconres.2009.08.032.

[18] J. Assaad, K.H. Khayat, H. Mesbah, Assessment of thixotropy of flowable and self-consolidating concrete, ACI Mater. J. 100(2) (2003) 99-107.

[19] P. Billberg, Form pressure generated by self-compacting concrete, in: Proceedings of the 3rd international RILEM symposium on self-compacting concrete, RILEM PRO33 Reykjavik, Iceland, 2003 271-280.

[20] P. Mounanga, K. Cherkaoui, A. Khelidj, M. Courtial, M.N. de Noirfontaine, F. Dunstetter, Extrudable reactive powder concretes: hydration, shrinkage and transfer properties, European Journal of Environmental and Civil Engineering 16(sup1) (2012) 99-114. https://doi.org/10.1080/19648189.2012.681961.

[21] O. Bonneau, C. Vernet, M. Moranville, P.C. Aïtcin, Characterization of the granular packing and percolation threshold of reactive powder concrete, Cem. Concr. Res. 30(12) (2000) 1861-1867. https://doi.org/10.1016/S0008-8846(00)00300-8.

[22] A. Tafraoui, G. Escadeillas, S. Lebaili, T. Vidal, Metakaolin in the formulation of UHPC, Constr. Buil. Mat. 23(2) (2009) 669-674. https://doi.org/10.1016/j.conbuildmat.2008.02.018.

[23] NF EN 197-1, Standard: Cement - Partie 1: Composition, specifications and conformity criteria for common cements (2012).

663 [24] H.H.C. Wong, A.K.H. Kwan, Packing density of cementitious materials: part 1-measurement
664 using a wet packing method, Materials and Structures 41 (2008) 689-701.
665 https://doi.org/10.1617/s11527-007-9274-5.
666 [25] J.M. Mechling, A. Lecomte, K. Merriaux, Measurement of the absorption of water of the mineral
667 admixtures in concrete by evaporometry, Materials and Structures 36 (2003) 32-39.
668 https://doi.org/10.1007/BF02481568.
669 [26] NF EN 206, Standard: Concrete - Specification, performance, production and conformity (2014).
670 [27] E. Nguyen Amanjean, T. Vidal, Low cost Ultra-High Performance Fibre Reinforced Concrete
671 (UHPFRC) with flash metakaolin, Key Engineering Materials 629 (2014) 55-63.
672 doi:10.4028/www.scientific.net/KEM.629-630.55.
673 [28] K. Wille, A.E. Naaman, G.J. Parra-Montesinos, Ultra-high performance concrete with
674 compressive strength exceeding 150 MPa (22 ksi): a simpler way, ACI Mater. J. 108(1) (2011) 46-
675 54.
676 [29] NF EN 12350-7, Testing fresh concrete – Part 7: Air content - Pressure methods (2012).
677 [30] R. Yu, P. Spiesz, H.J.H. Brouwers, Mix design and properties assessment of Ultra-High
678 Performance Fibre Reinforced Concrete (UHPFRC), Cem. Concr. Res. 56 (2014) 29-39.
679 https://doi.org/10.1016/j.cemconres.2013.11.002.
680 [31] B. A. Graybeal, Material property characterization of ultra-high performance concrete, (2006), No.
681 FHWA-HRT-06-103.
682 [32] C. Legrand, Contribution to the study of the fresh concrete rheology, Materials and structures 5(5)
683 (1972) 275-295.
684 [33] NF EN 12350-2, Standard: Tests for fresh concrete - Part 2: Slump test (2012).
685 [34] P. Estellé, C., Lanos, A. Perrot, Processing the Couette viscometry data using a Bingham
686 approximation in shear rate calculation, Journal of Non-Newtonian Fluid Mechanics 154(1) (2008)
687 31-38. https://doi.org/10.1016/j.jnnfm.2008.01.006.
688 [35] G. Ovarlez, Introduction to the rheometry of complex suspensions, in: N. Roussel (Ed.),
689 Understanding the rheology of concrete, Woodhead Publishing Limited, 2012, Chapter 2.
690 [36] M. Bousmina, A. Aït-Kadi, J.B. Faisant, Determination of shear rate and viscosity from batch
691 mixer data, Journal of Rheology 43 (1999) 415-433. https://doi.org/10.1122/1.551044.
692 [37] G. Heirman, L. Vandewalle, D. Van Gemert, O. Wallevik, Integration approach of the Couette
693 inverse problem of powder type self-compacting concrete in a wide-gap concentric cylinder

694 rheometer, Journal of Non-Newtonian Fluid Mechanics 150 (2008) 93–103.
695 https://doi.org/10.1016/j.jnnfm.2007.10.003.
696 [38] C. Anglade, A. Papon, M. Mouret, Constitutive parameter identification: an application of inverse
697 analysis to the flow of cement-based suspensions in the fresh state from synthetic data, Journal of
698 Non-Newtonian Fluid Mechanics 241 (2017) 14-25. https://doi.org/10.1016/j.jnnfm.2017.01.005.
699 [39] D.J. Sheskin, Handbook of parametric and nonparametric statistical procedures, 3rd ed. Chapman
700 & Hall/CRC, 2004.
701 [40] N. Roussel, Correlation between yield stress and slump: comparison between numerical
702 simulations and concrete rheometers results, Materials and Structures 39(4) (2006) 501-509.
703 https://doi.org/10.1617/s11527-005-9035-2.
704 [41] A.A. Hassan, M. Lachemi, K.M. Hossain, Effect of metakaolin and silica fume on rheology of
705 self-consolidating concrete, ACI Mater. J. 109(6) (2012) 657-664.
706 [42] A.A. Ramezanianpour, Cement replacement materials, Springer-Verlag, Berlin Heidelberg (2014).
707 [43] S. Grünewald, Fibre reinforcement and rheology of concrete, in: N. Roussel (ed.), Understanding
708 the rheology of concrete, Woodhead Publishing Limited, Chapter 9, 2012.
709 [44] O.H. Wallevik, Rheology–a scientific approach to develop self-compacting concrete, in: O.
710 Wallevik, I. Nielsson (Eds.), International RILEM Symposium on Self-Compacting Concrete,
711 RILEM Publications SARL, 2003, pp. 23–31.
712 [45] F. de Larrard, Concrete mixture proportioning - a scientific approach, E&FN SPON, 1999.
713 [46] M. Cyr, M. Mouret, Rheological characterization of superplasticized cement pastes containing
714 mineral admixtures: consequences on self-compacting concrete design, in V.M. Malhotra (ed),
715 Proceedings SP-217 of the 7th CANMET/ACI International Conference on superplasticizers and other
716 chemical admixtures in concrete, Berlin, 2003, American Concrete Institute, pp. 241-256.
717 [47] I.P. Sfikas, E.G. Badogiannis, K.G. Trezos, Rheology and mechanical characteristics of self-
718 compacting concrete mixtures containing metakaolin, Constr. Buil. Mat. 64 (2014) 121-129.
719 https://doi.org/10.1016/j.conbuildmat.2014.04.048.
720 [48] J.E. Wallevik, Thixotropic investigation on cement paste: experimental and numerical approach,
721 Journal of Non-Newtonian Fluid Mechanics 132 (1-3) (2003) 86–99.
722 https://doi.org/10.1016/j.jnnfm.2005.10.007.
723 [49] G. Ovarlez, N. Roussel, A physical model for the prediction of lateral stress exerted by self-
724 compacting concrete on formwork, Materials and Structures 39(2) (2006) 269-279.
725 https://doi.org/10.1617/s11527-005-9052-1.

726 [50] P. Billberg, Development of SCC static yield stress at rest and its effect on the lateral form
727 pressure, in: SCC 2005, Combining the Second North American Conference on the Design and Use
728 of Self-Consolidating Concrete and the Fourth International RILEM Symposium on Self-
729 Compacting Concrete, 2005, 583-589.
730 [51] H.A. Barnes, Thixotropy - a review, Journal of Non-Newtonian Fluid Mechanics 70(1-2) (1997) 1-
731 33. https://doi.org/10.1016/S0377-0257(97)00004-9.
732 [52] R.S. Ahari, T.K. Erdem, K. Ramyar, Time-dependent rheological characteristics of self-
733 consolidating concrete containing various mineral admixtures, Constr. Buil. Mat. 88 (2015) 134-
734 142. https://doi.org/10.1016/j.conbuildmat.2015.04.015.
735 [53] A. Carneiro, M. Mouret, Flow properties of fluid concretes incorporating or not metakaolin, in: A.
736 Palomo, A. Zaragoza, J.C. Lopez Agui (Eds.), Paper 427, area 7 (properties of fresh and hardened
737 concrete), CD Proceedings of the 13th International Congress on the Chemistry of Cement, Madrid,
738 July 2011, 3-8.
739 [54] J. Assaad, K.H. Khayat, H. Mesbah, Variation of formwork pressure with thixotropy of self-
740 consolidating concrete, ACI Mater. J. 100(1) (2003), 29-37.
741 [55] K. Khayat, J. Assaad, H. Mesbah, M. Lessard, Effect of section width and casting rate on
742 variations of formwork pressure of self-consolidating concrete, Materials and structures 38(1)
743 (2005) 73-78. https://doi.org/10.1007/BF02480577.
744 [56] NF EN 12350-6, Testing fresh concrete - Part 6: Density (2012).
745 [57] A.W. Saak, H.M. Jennings, S.P. Shah, New methodology for designing self-compacting concrete,
746 Materials Journal 98(6) (2001) 429-439. doi:10.1617/14074.